THE JOURNAL OF PHYSICAL CHEMISTRY C

Article

pubs.acs.org/JPCC

Graphene Oxide as a Practical Solution to High Sensitivity Gas Sensing

Stefano Prezioso,*[,†] Francesco Perrozzi,[†] Luca Giancaterini,[‡] Carlo Cantalini,[‡] Emanuele Treossi,[§,∥] Vincenzo Palermo,[§] Michele Nardone,[†] Sandro Santucci,[⊥] and Luca Ottaviano[†]

[†]Dipartimento di Scienze Fisiche e Chimiche, Università dell'Aquila, Via Vetoio, 67100, L'Aquila, Italy

[‡]Dipartimento di Ingegneria Industriale e dell'Informazione e di Economia, Università dell'Aquila, Via Gronchi 18, 67100, L'Aquila, Italy

[§]CNR-ISOF, Via Gobetti 101, 40129 Bologna, Italy

[∥]Laboratorio MIST.E-R, Via Gobetti 101, 40129 Bologna, Italy

[⊥]Dipartimento di Science Fisiche e Chimiche, Università dell'Aquila, gc-LNGS INFN, Via Vetoio, 67100, L'Aquila, Italy

Supporting Information

ABSTRACT: Graphene and its related materials have attracted much interest in sensing applications because of their optimized ratio between active surface and bulk volume. In particular, several forms of oxidized graphene have been studied to optimize the sensing efficiency, sometimes moving away from practical solutions to boost performance. In this paper, we propose a practical, high-sensitivity, and easy to fabricate gas sensor based on high quality graphene oxide (GO), and we give the rationale to the high performance of the device. The device is fabricated by drop-casting water-dispersed single-layer GO flakes on standard 30 μm spaced interdigitated Pt electrodes. The exceptional size of the GO flakes (27 μm mean size and ~500 μm maximum size) allows single GO flake to bridge adjacent electrodes. A typical p-type response is observed by testing the device in both reducing and oxidizing environments. The specific response to NO_2 is studied by varying the operating temperature and the gas concentration. Sensing activity is demonstrated to be mainly mediated by the oxygen functional groups. A 20 ppb detection limit is measured. Besides illustrating a simple and efficient approach to gas sensing, this work is an example of the versatility of graphene oxide, accomplishing tasks that are complementary to graphene.

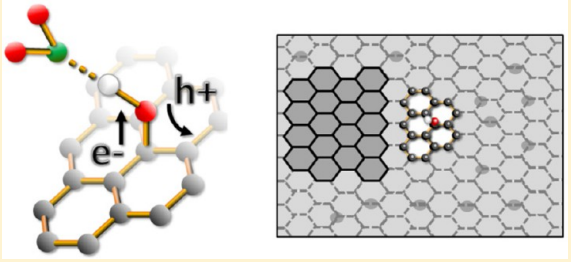

INTRODUCTION

Graphene with its derivatives is the most versatile material that has ever been discovered.[1] Just to cite some unusual examples of graphene applications, we can mention its use as a catalyst,[2] as an antibacterial agent,[3] or as a tool for fast DNA sequencing.[4] Yet, due to its easily tunable electronic properties, graphene has been widely employed in electronic applications.[5] Novoselov et al.[6] were the first reporting in 2004 about the fabrication of a graphene-based field effect transistor and many other works followed showing improvement of the device performance.[7,8] More recently, starting from the pivotal work of Gunlycke at al.[9] many studies have been devoted to demonstrate practical memory devices employing graphene[10] or its related materials.[11,12] Light absorption properties have been even more recently reported showing the way forward to applications in photovoltaics.[13] At the same time, the increasing demand on the fabrication of patterned graphene-based films for applications in miniaturized electronics and integrated circuit technologies has stimulated the advance in the lithographic techniques, on the wake of the Si-based technology.[14,15]

Due to the large specific area of graphene-based materials, their use in sensing applications is one of the hot topics in graphene literature. Sensing is intended in the literature in its extended meaning, many works reporting on gas sensing as well as on biosensing applications, such as pH and protein detection,[16,17] DNA detection,[4,18] electrochemical biosensing of glucose,[19] immunosensing,[20] and real-time detection of molecules released from living cells.[21] Nonetheless, a big interest is definitely still reserved to gas sensing.[22] The enormous potential of graphene as a gas sensing material was figured out in 2004 as Novoselov et al.[6] reported on the doping effect observed under water and ethanol vapors exposure. Starting from this work, Schedin et al.[23] demonstrated the detection of individual gas molecules adsorbed on graphene. Encouraged by this pivotal result, many other works followed to investigate practical solutions to optimize gas detection and selectivity. Theoretical works have agreed on the fact that functionalization of graphene is the best way to improve sensing performance, gas molecules being weakly adsorbed on pristine graphene and more strongly on doped or defective

Received: August 29, 2012
Revised: April 18, 2013
Published: April 25, 2013

dx.doi.org/10.1021/jp3085759 | J. Phys. Chem. C 2013, 117, 10683−10690

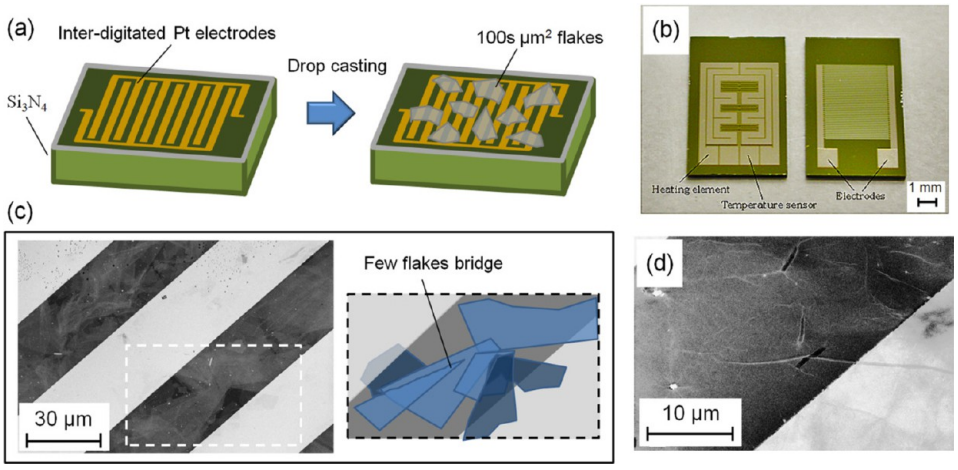

Figure 1. (a) Sketch of the device fabrication. Electric contacts between prepatterned interdigitated Pt electrodes are realized upon drop-casting deposition of large GO flakes. (b) Patterned substrate (front-size) with heating elements and temperature sensors on the backside. (c) SEM image of few GO flakes bridging two adjacent Pt electrodes. (d) SEM image of a GO flake lying over an electrode edge.

graphene.[24−26] Functionalization can be achieved in different ways, each one with pros and cons. The use of graphene oxide (GO) has been universally recognized as the handiest way to functionalize graphene because it is easy to process and to modify subsequently. To date, modified GO rather than GO has been used in prototype sensors because of the need of balancing the reactivity to gas molecules that increases with the number of active sites and the detrimental effect of these sites on the electric transport. Chemically and thermally reduced GO has been used with excellent results.[27−31] GO has been also functionalized with additional molecules[32,33] or decorated with nanoparticles to be more selective.[34] Yet, performance has been further somewhat improved using micro- and nanostructured GO.[35−37]

The challenge today is to move from a prototype to a practical device.[28,38,39] Up to now, most of the strategies aimed to improve the device performance have moved far from practical solutions, because based on the established idea that the more advanced is the GO refining process the higher is the performance of the final device without considering the possibility of just improving the starting material. Here, we propose a practical high-sensitivity gas sensor based on high quality GO. The device fabrication simply consists in drop-casting water dispersed single GO flakes on standard 30 μm spaced interdigitated Pt electrodes. Flakes are large enough to make single flake bridge between adjacent electrodes with consequent optimization of the electrical contacts. The device has been tested with NO_2. The detection limit measured with NO_2 is 20 parts-per-billion (ppb), that is the lowest value ever measured with practical graphene-based sensors to the best of our knowledge.[40−42] Lower detection resolutions (down to ∼1 ppb detection limit) are today allowed only by single graphene flake devices, exemplary demonstrations of technological excellence, but, due the limits of the up-to-date manufacturing processes, far from representing practical solutions to high sensitivity gas sensing.[23] A model of gas sensing is proposed on the basis of the theory reported in the literature,[43] that assigns the sensing activity to the oxygen functional groups at the GO surface.

EXPERIMENTAL SECTION

Material Preparation. GO is prepared via a modified Hummers method[44] starting from graphite flakes of 500 μm maximum size. Monolayers with ∼30 μm average size (about 2 orders of magnitude higher than for commercial GO) and 1.1 ± 0.1 nm thickness[45] are obtained and dispersed in water for eventual deposition. The exceptional size of flakes is of strategic importance to the aims of our work.

Device Fabrication. The water dispersed GO is deposited by 80 μL drop-casting on 30 μm spaced interdigitated Pt electrodes patterned on Si_3N_4 substrate. The drop-casted GO solution is air-dried at 50 °C. No additional procedures are needed. The small effort required to fabricate a so high performance device is the strong point of our work, making GO a practical solution to high sensitivity gas sensing.

Material Characterization. A scanning electron microscope (SEM) (ZEISS-GEMINI LEO 1530) has been used to observe the GO flakes. SEM analysis, aimed to study the size distribution of GO, has been performed on scattered flakes deposited by 2000 rpm spin-coating on 300 nm SiO_2/Si(100) substrate. Room temperature micro-Raman spectroscopy (μRS) has been performed with a LABRAM spectrometer (Horiba-Jobin Yvon, λ = 633 nm, 1 μm spatial resolution, and ∼2 cm^{-1} spectral resolution) equipped with a confocal optical microscope (100× MPLAN objective with 0.9 numerical aperture and 0.15 mm work distance). GO investigated by μRS has been deposited by spin-coating on 72 nm Al_2O_3/Si(100) for best optical identification of flakes.[46] X-ray photoemission spectroscopy (XPS) has been performed with a PHI 1257 spectroscometer (monochromatic Al K_α source, $h\nu$ = 1486.6 eV, base pressure 2×10^{-10} Torr). GO investigated by XPS has been deposited by spin coating on Au(100) substrate. Prior to the deposition, the Au(100) surface has been chemically cleaned with NH_4−OH 25% in H_2O_2. The thickness of the deposited GO film (∼ 10 nm) results from a trade-off between the maximization of the signal from GO and the minimization of the charging effects due to its dielectric behavior.

Sensing Test. The electrical response of the device has been studied by varying the operating temperature (OT) in the 25−200 °C range. Volt-amperometric measurements have been performed with a Keithley 2001 multimeter, forcing 4.4 nA into

dx.doi.org/10.1021/jp3085759 | J. Phys. Chem. C 2013, 117, 10683−10690

the device. Resistance variations have been recorded under alternating exposure to dry air and NO_2. Different gas concentrations have been obtained in the 20 ppb to 10 ppm range by controlled dilution of NO_2 in dry air. Gas has been fluxed into the chamber containing the sensor under a continuous and constant regime. Chamber pressure was fixed at 1 bar. The device temperature has been controlled by heating elements and temperature sensors (thermocouples) integrated on the device backside, guaranteeing that the gas pressure was not affected by the changes in the OT. The device response has been estimated via the following parameter

$$\Delta R(\%) = \frac{|R_A - R_G|}{R_A + R_G} \times 100$$

where R_G is the device resistance in the presence of the target gas and R_A is the one in dry air. Response time has been calculated as the time required for the device resistance to change by a factor of 90% of $|R_A - R_G|$.

RESULTS AND DISCUSSION

Figure 1a schematically shows the basics of the device fabrication. Thirty micrometer-spaced interdigitated Pt electrodes are patterned on Si_3N_4 substrate. Figure 1b shows a picture of the patterned texture (front-size) with heating elements and temperature sensors on the back-side. GO flakes are deposited on the patterned substrate by 80 μL drop-casting to make electric contacts between adjacent electrodes. In Figure 1c we report a SEM image showing a typical interelectrodes bridge where the electric contact is obtained with few GO flakes. The schematic view helps the identification of the flakes in the dashed line marked area. Figure 1d shows the detail of a single GO flake lying over an electrode edge.

In Figure 2 we report a large-field SEM image showing scattered GO flakes deposited by spin coating on 300 nm SiO_2/Si(100) substrate with the aim of a flakes size distribution analysis. The inset of Figure 2 reports such a size distribution as

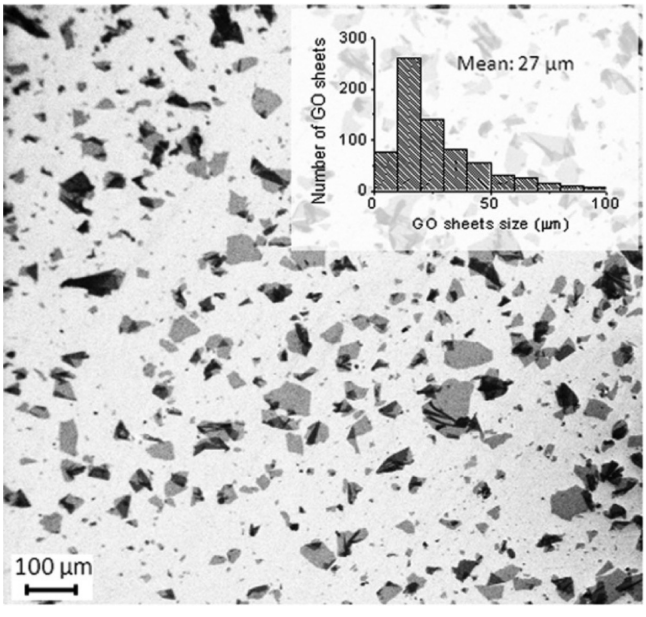

Figure 2. SEM image of GO sheets deposited by 2000 rpm spin-coating on 300 nm SiO_2/Si(100) substrate. Inset: GO flakes size distribution. The mean size is 27 μm.

obtained from the SEM image. The distribution is log-normal. The average size is 27 μm, i.e., very close to the 30 μm spacing between Pt electrodes. With this size distribution, a single flake interelectrode bridge is a favored configuration.

GO has been characterized both by XPS and room-temperature μRS. Analysis has been extended to GO annealed at 200 °C in ultrahigh vacuum (UHV) to monitor the evolution of the chemical bonds in the OT range (0−200 °C) in the absence of contaminants. In Figure 3 we report the XPS C1s

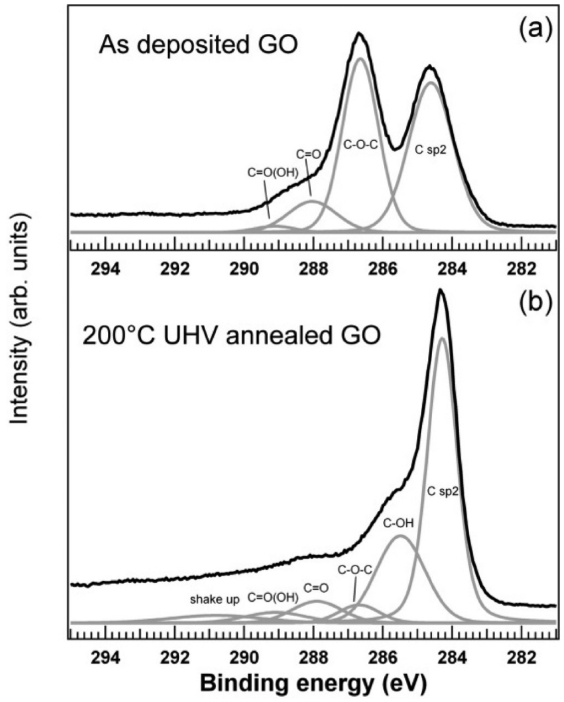

Figure 3. XPS C1s core level spectra of as deposited GO (a) and 200 °C UHV annealed GO (b). Both spectra are fitted by the sum of five components: C=C/C−C (C−H) (284.6−284.9 eV), C−OH (285.9 eV), C−O−C (286.9 eV), C=O (288.0 eV), C=O(OH) (289.3 eV), and the $\pi-\pi^*$ shakeup component (290.6 eV).

core-level spectra of as-deposited GO (a) and 200 °C UHV annealed GO (b). Both C1s spectra are nicely fitted by the sum of five components assigned (in line with the literature[47−50]) to C atoms belonging to aromatic rings and hydrogenated carbon (C=C/C−C, C−H, 284.6−284.9 eV), hydroxyl groups (C−OH, 285.9 eV), epoxy groups (C−O−C, 286.9 eV), carbonyl groups (C=O, 288.0 eV), and carboxyl groups (C=O(OH), 289.3 eV) (the hump at 290.6 eV is assigned to a $\pi - \pi^*$ shakeup satellite[51]). As a consequence of thermal annealing, all the groups containing oxygen tend to disappear, unlike those containing carbon only (aromatic groups), indicating a loss of oxygen in favor of sp^2 carbon domains formation.

In Figure 4 we report the μRS spectra measured for as-deposited GO (solid line) and 200 °C UHV annealed GO (dashed line). The substrate used for μRS analysis was 72 nm Al_2O_3/Si(100) for best optical identification of flakes.[46] Both spectra have the characteristic shape of GO. The two peaks (at ~1330 cm^{-1} and ~1600 cm^{-1}) are respectively assigned to the D band, commonly related to defects (edges included), and the G band, characteristic of graphene.[52] Both spectra are normalized to the G peak intensity. As a consequence of thermal reduction, the ratio I_D/I_G between the D peak and G peak intensities decreases. In particular, I_D/I_G passes from 1.37

dx.doi.org/10.1021/jp3085759 | J. Phys. Chem. C 2013, 117, 10683−10690

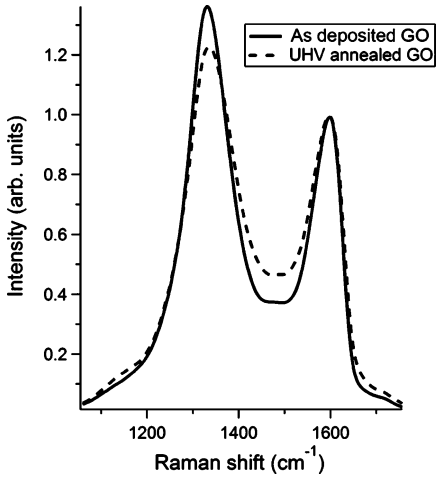

Figure 4. Room-temperature μRS of GO before (solid line) and after thermal annealing at 200 °C in UHV (dashed line).

to 1.24. Using the Tunistra–Koenig equation,[53] we obtain that, correspondingly, the average size L_a of sp^2 carbon domains passes from 6.1 to 6.3 nm (i.e., ~ 3% L_a increase). This is in line with the formation of sp^2 carbon domains observed by XPS. For completeness, the whole Raman spectrum with the 2D and D+G peaks is reported in Section 1 of the Supporting Information.

The electrical response of our device has been preliminary tested in dry air at different temperatures, namely, at 150 and 200 °C. In both cases, the device has been tested over 10s hours operation time. The plot of the device resistance versus time is reported in Figure 5, where the blue line refers to the

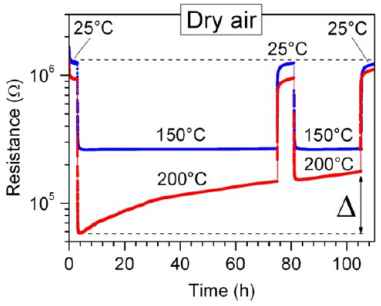

Figure 5. Electrical response over a long time scale (>100 h) to 25–150 °C cycles (blue line) and 25–200 °C cycles (red line) in dry air. Δ represents the overall variation of resistance at 200 °C.

25–150 °C cycles, while the red line refers to the 25–200 °C ones. The first important outcome of this test is that in neither case is device degradation observed, despite the very long working time. As a matter of fact, when the OT has been kept below 200 °C, the device has worked for thousands of hours without manifesting any sign of degradation other than a gradual decrease of resistance due to a progressive heating-induced reduction of the GO film that usually stops when the 150 °C-equivalent reduction degree is reached (if 150 °C is the maximum OT, as in our case). On the contrary, when the OT has exceeded 250 °C, a steep increase of the device resistance to open-circuit values has been observed just after a few minutes of operation, as shown in Section 2 of the Supporting Information. 200 °C OT is a threshold temperature between stable operating conditions and the breaking state. At 200 °C the device is not stable as at 150 °C, its resistance drifting from 6×10^4 Ω at the beginning of the test (i.e., as soon as the temperature step is applied) to 2×10^5 Ω at the end of the test (i.e., just before the room temperature is recovered) but, at the same time, a 200 °C cycle has never been observed to induce GO film rupture. As reported in detail in Section 3 of the Supporting Information, the drift of the resistance value at 200 °C OT can be ascribed to a loss of material, generally observed above 180 °C. The information we obtain from this test of stability is that sensing operations have to be performed at 150 °C maximum OT (data reported in Section 6 of the Supporting Information indicate, at the same time, that lower OTs are not recommended because the response is much slower). 150 °C is also the activation temperature (AT) for a pristine device. The AT is studied in Section 4 of the Supporting Information where we report the electrical response to NO_2 measured during the starting operations of two different pristine devices, one fabricated with as-deposited GO, and the other one with 300 °C UHV annealed GO. We observe that the as-deposited GO device becomes conductive and, hence, sensitive to the gas at 150 °C, that is, its AT, while the 300 °C UHV annealed GO device is perfectly working just from the first operations at room temperature (the same is if UHV annealing is performed at 200 °C). In Section 5 of the Supporting Information we report a study of resistance as a function of the OT in the 50–150 °C range showing that the mechanism of carrier transport is hopping, in agreement with the literature.[54,55] As a corollary of this latter evidence, the Schottky contribution due to the electric contacts can be considered negligible, as in ref 55.

Tests at fixed 150 °C temperature in both oxidizing and reducing environment are reported in Figure 6. The device has

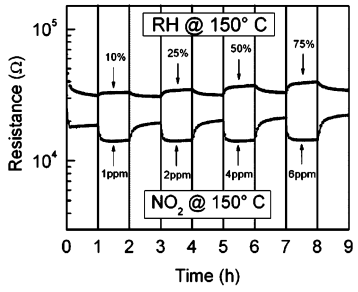

Figure 6. Electrical response to humidity at 150 °C (RH = 10%, 25%, 50%, and 75%) and to NO_2 at 150 °C (1 ppm, 2 ppm, 4 ppm, and 6 ppm NO_2).

been exposed to increasing relative humidity (RH) (reducing environment) and increasing NO_2 concentration (oxidizing environment). The response is typical of a p-type sensor, like the one observed for carbon nanotubes.[56] The device resistance is, in fact, increased upon exposure to reducing agents, while it decreases in an oxidizing environment. The same behavior has been more recently reported for chemically derived graphene.[28] The device response is enhanced by the increase of gas (or vapor) flow.

The detection of NO_2 has been studied as a function of the OT in the 25–150 °C range (Figure 7). The device has been exposed to a cycle consisting, for one-half, of steps at increasing OT up to 150 °C (namely 25 °C, 50 °C, 100 °C, and 150 °C) and, for the other half, of steps at decreasing OT down to room temperature (namely 150 °C, 100 °C, 50 °C, and 25 °C). Each step (lasting 3 h) consists of 1 h exposure to dry air, 1 h exposure to 5 ppm NO_2, and again 1 h exposure to dry air. The

dx.doi.org/10.1021/jp3085759 | J. Phys. Chem. C 2013, 117, 10683–10690

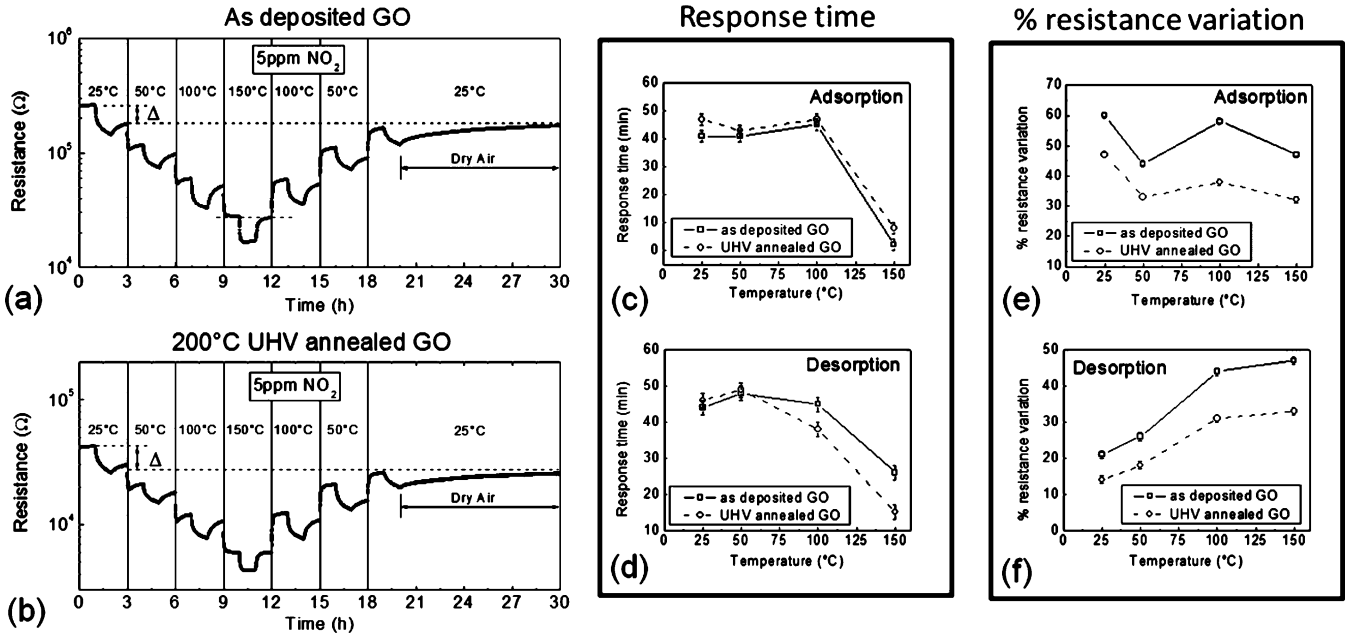

Figure 7. Electrical response at different temperatures (25−50−100−150−100−50 °C cycle) of the as deposited GO (a) and 200 °C UHV annealed GO device (b) to 5 ppm NO_2 in dry air. Each step (lasting 3 h) consists of 1 h exposure to dry air, 1 h exposure to 5 ppm NO_2, and again 1 h exposure to dry air. Absorption (c) and desorption (d) response times of the as-deposited GO (solid lines) and UHV annealed GO device (dashed lines) as a function of the working temperature. Absorption (e) and desorption (f) percentage resistance variation of the as-deposited GO (solid lines) and UHV annealed GO device (dashed lines) as a function of the working temperature. Data of panels c−f have been obtained from panels a and b.

final step has been prolonged to allow the complete recovering of the room temperature resistance. The response curve is reported in Figure 7a. The same has been done for a second device with GO annealed at 200 °C in UHV. The response curve of this new device is reported in Figure 7b. In both cases, the curve is almost symmetric with respect to the 150 °C step, indicating that the device history has negligible effects on its performance. A lower baseline resistance (i.e., the one measured at 25 °C before beginning the experiment) is measured in the case of the annealed GO (4.2×10^4 Ω vs 2.6×10^5 Ω for as deposited GO) because of the thermal reduction. In both cases, the baseline resistance decreases after a complete cycle by an amount Δ that is, respectively, the 40% (as deposited GO) and 47% (annealed GO) of the initial value, due to a systematic more efficient gas adsorption than desorption.

A quantitative comparison between panels a and b of Figure 7 is summarized in panels c−f. In all these panels, the solid line refers to as deposited GO, while the dashed line refers to UHV annealed GO. Panels c and d report, respectively, the values of adsorption and desorption response time as a function of the OT. In both cases, the response time decreases as the OT increases. Plots in panel c almost overlap over the whole OT range, indicating that the adsorption kinetics is comparable in the two devices. The same is true for the plots in panel d up to 50 °C. At higher OTs, desorption becomes faster for annealed GO, which is in line with the improved kinetics observed by other authors at increasing GO reduction degree.[27] What is even more relevant is the absolute value of response time at 150 °C OT, that is, a few minutes in adsorption and a few tens of minutes in desorption. The smallest value here measured is 2 min (namely, the adsorption response time of the as-deposited GO device), a value that makes our work competitive with many other works in the literature. Panels e and f report, respectively, the values of adsorption and desorption percentage resistance variation, $\Delta R(\%)$, as a function of the OT. $\Delta R(\%)$ is calculated from the respective curves in panels a and b as the ratio between the total resistance variation in each single adsorption (desorption) step and the mean resistance value across that step. While no clear effects of temperature can be observed in the case of adsorption, a response enhancement is definitely recorded in the case of desorption as the OT is increased ($\Delta R(\%)$ more than doubles). Data reported in panels c and f, i.e., those referring to desorption, show a trend from smaller response and slower response times at room temperature to larger response and faster response times at higher temperature. In terms of response time, this behavior is analogous to the one of highly reduced GO,[28] while the enhanced response at higher OTs is an effect of the increased atomic vibrations that favor the removal of the adsorbed molecules from the active sites.

Besides showing a simple overall temperature dependent trend, panels e and f also show a remarkable difference between as-deposited GO and annealed GO device responses. Quantitatively, the ratio $\Delta R_{GO}/\Delta R_{GO\text{-}ann}$ between GO and annealed GO curves (respectively, solid and dashed line) is systematically larger than unit, indicating that as-deposited GO is in general more reactive to gas molecules than annealed GO (the same holds true if $\Delta G_{GO}/\Delta G_{GO\text{-}ann}$ is used, with $G = 1/R$). This has already been predicted in the literature.[24−26] In particular, the sensing activity of the oxygen functional groups in GO has been described in detail.[43] In Table 1 we report adsorption and desorption values of $\Delta R_{GO}/\Delta R_{GO\text{-}ann}$ as a function of the annealing temperature.

Data reported in Table 1 show that, both in adsorption and desorption, $\Delta R_{GO}/\Delta R_{GO\text{-}ann}$ increases as the annealing temperature increases. Since we know, on the basis of data reported in ref 50, where we have studied the effects of thermal annealing on our GO, that the density of oxygen functional groups

dx.doi.org/10.1021/jp3085759 | J. Phys. Chem. C 2013, 117, 10683−10690

Table 1. $\Delta R_{GO}/\Delta R_{GO\text{-}ann}$ Values for As-Deposited, 200°C and 300°C UHV Annealed GO, Both in Adsorption and Desorption[a]

$\Delta R_{GO}/\Delta R_{GO\text{-}ann}$	as dep. GO	200 °C ann. GO	300 °C ann. GO
adsorption	1[b]	1.5	1.7
desorption	1[b]	1.4	1.6

[a]Data reported in Figure 7 and Figure S4 of the Supporting Information have been used to obtain these values. [b]By definition.

decreases as the annealing temperature increases, data of Table 1 can be also read in the following way: both in adsorption and desorption, $\Delta R_{GO}/\Delta R_{GO\text{-}ann}$ increases as the density of functional groups, due to annealing, decreases. This is the same as saying that sensitivity decreases as the density of functional groups decreases. Hence, we can here definitively attribute to these groups the important role of gas-sensing active sites.

To be thorough, the as-deposited GO we refer hereto is not pristine because it has been reduced (in air) during the first sensing operations at 150 °C (see Section 4 of the Supporting Information). Nonetheless, an extra amount of oxygen functional groups is present in the as deposited GO with respect to the 200 °C annealed GO (see Figure S5 of Supporting Information), which justifies the higher sensitivity of GO if not annealed.

The gas sensing mechanism described in ref 43 is consistent with all the experimental results here reported. NO_2 molecules are mainly adsorbed by the oxygen functional groups. In correspondence to the active sites, a negative charge, usually fractions of the electronic charge, is transferred to the NO_2 molecule with consequent generation of a positively charged vacancy in the honeycomb structure underneath, giving reason for the p-type-like behavior. Nevertheless, here we are not excluding that adsorption may occur also in correspondence to the graphene patches where an analogous doping effect is induced,[57] even enhanced by the intrinsic quantum capacitance of graphene.[58] Yet, the graphene contribution to sensitivity may be enhanced by the presence of intercalated/adsorbed water molecules serving as dipoles.[59]

In Figure 8 the GO response at 150 °C is reported for different NO_2 concentrations. The device resistance is monitored in the time. Starting from 20 ppb, the NO_2 concentration is increased up to 10 ppm with finite steps (40 ppb, 100 ppb, 200 ppb, 400 ppb, 800 ppb, 1 ppm, 2 ppm, 5 ppm, 8 ppm, and 10 ppm). Each step consists of 1 h exposure to NO_2 (adsorption) and 1 h exposure to dry air (desorption). The detection limit is 20 ppb (bottom-left inset), that is the lowest value ever measured with graphene based sensors.[40−42] The same detection limit has been measured at room temperature (see Section 6 of the Supporting Information for more details). The corresponding sensitivity curve (0.5 slope) is reported in the top-right inset. The very low detection limit can be ascribed, on the one hand, to the high number of active oxygen sites and, on the other hand, to the optimized signal-to-noise ratio achieved with the use of high quality GO. At the same time, the high number of oxygen functional groups has a detrimental effect on the response time, that is, a few minutes (at 150 °C OT) versus the potential few seconds response time of highly reduced GO-based devices.[27] These results suggest that GO is an excellent material for gas sensing. In particular, it is the right choice to fabricate low-cost sensors with high sensitivities and moderately fast responses.

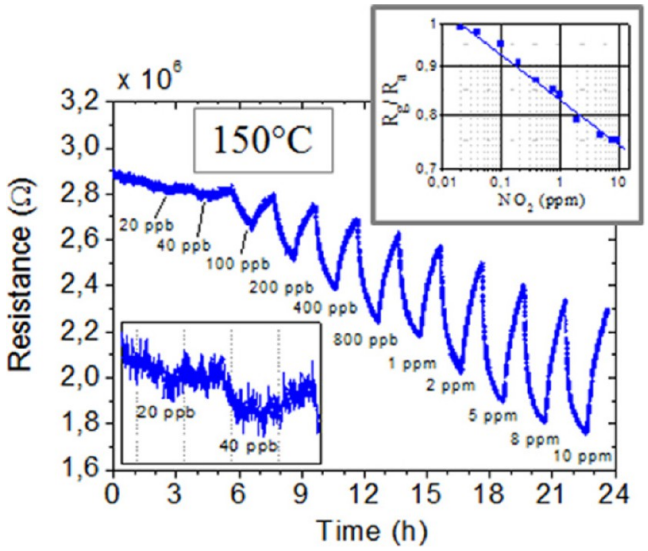

Figure 8. GO response to increasing NO_2 concentration at 150 °C OT. Device resistance versus time is reported in the main panel. Bottom-left inset: zoom in the detection limit range. Top-right inset: sensitivity curve.

CONCLUSIONS

In conclusion, we have demonstrated a practical p-type gas sensor using GO drop-casted on standard interdigitated Pt electrodes. Our device is stable, has a lifetime larger than 1000s hours, and exhibits a very low detection limit (20 ppb). The excellent performance is due to the high quality of our GO (large and highly oxidized flakes). With respect to other relevant cases in the literature, such as highly reduced GO and carbon nanotubes, GO has the advantage to have a much larger number of active sites but the limitation to be poorly conductive. Because of this, GO is a good choice for applications that do not need fast responses but require high sensitivities. We believe that this work will promote the use of GO for the easy and low-cost fabrication of highly versatile (e.g., transparent and flexible devices) and environmentally friendly gas sensors.

ASSOCIATED CONTENT

Supporting Information

Graphene oxide film rupture conditions. Study of the device instability at 200 °C OT. Dependence of device resistance on the OT and associated transport model. This material is available free of charge via the Internet at http://pubs.acs.org.

AUTHOR INFORMATION

Corresponding Author

*E-mail: stefano.prezioso@aquila.infn.it.

Notes

The authors declare no competing financial interest.

ACKNOWLEDGMENTS

This work was supported by "Programma Operativo FESR 2007-2013 della Regione Emilia-Romagna − Attività I.1.1.", by the European Science Foundation (ESF) under the EURO-CORES Program EuroGRAPHENE (GOSPEL), and by the EC Marie-Curie ITN-GENIUS (PITN-GA-2010-264694). Authors acknowledge Dr. G. Profeta for the fruitful discussion on the gas sensing mechanism.

REFERENCES

(1) Geim, A. K. Graphene: Status and Prospects. *Science* **2009**, *324*, 1530−1534.

(2) Pyun, J. Graphene Oxide as Catalyst: Application of Carbon Materials Beyond Nanotechnology. *Angew. Chem., Int. Ed.* **2011**, *50*, 46−48.

(3) Hu, W.; Peng, C.; Luo, W.; Lv, M.; Li, X.; Li, D.; Huang, Q.; Fan, C. Graphene-Based Antibacterial Paper. *ACS Nano* **2010**, *4*, 4317−4323.

(4) Min, S. K.; Kim, W. Y.; Cho, Y.; Kim, K. S. Fast DNA Sequencing with a Graphene-Based Nanochannel Device. *Nat. Nanotechnol.* **2011**, *6*, 162−165.

(5) Huang, X.; Yin, Z.; Wu, S.; Qi, X.; He, Q.; Zhang, Q.; Yan, Q.; Boey, F.; Zhang, H. Graphene-Based Materials: Synthesis, Characterization, Properties, and Applications. *Small* **2011**, *7*, 1876−1902.

(6) Novoselov, K. S.; Geim, A. K.; Morozov, S. V.; Jiang, D.; Zhang, Y.; Dubonos, S. V.; Grigorieva, I. V.; Firsov, A. A. Electric Field Effect in Atomically Thin Carbon Films. *Science* **2004**, *306*, 666−669.

(7) Chen, Z.; Lin, Y.-M.; Rooks, M. J.; Avouris, P. Graphene Nano-Ribbon Electronics. *Physica E* **2007**, *40*, 228−232.

(8) Liao, L.; Bai, J.; Lin, Y.-C.; Qu, Y.; Huang, Y.; Duan, X. High-Performance Top-Gated Graphene-Nanoribbon Transistors Using Zirconium Oxide Nanowires as High-Dielectric-Constant Gate Dielectrics. *Adv. Mater.* **2010**, *22*, 1941−1945.

(9) Gunlycke, D.; Areshkin, D. A.; Li, J.; Mintmire, J. W.; White, C. T. Graphene Nanostrip Digital Memory Device. *Nano Lett.* **2007**, *7*, 3608−3611.

(10) Zheng, Y.; Ni, G.-X.; Toh, C.-T.; Zeng, M.-G.; Chen, S.-T.; Yao, K.; Özyilmaz, B. Gate-Controlled Nonvolatile Graphene-Ferroelectric Memory. *Appl. Phys. Lett.* **2009**, *94*, 163505.

(11) He, C. L.; Zhuge, F.; Zhou, X. F.; Li, M.; Zhou, G. C.; Liu, Y. W.; Wang, J. Z.; Chen, B.; Su, W. J.; Liu, Z. P. Nonvolatile Resistive Switching in Graphene Oxide Thin Films. *Appl. Phys. Lett.* **2009**, *95*, 232101.

(12) Wang, S.; Pu, J.; Chan, D. S. H.; Cho, B. J.; Loh, K. P. Wide Memory Window in Graphene Oxide Charge Storage Nodes. *Appl. Phys. Lett.* **2010**, *96*, 143109.

(13) Yan, X.; Cui, X.; Li, B.; Li, L.-S. Large, Solution-Processable Graphene Quantum Dots as Light Absorbers for Photovoltaics. *Nano Lett.* **2010**, *10*, 1869−1873.

(14) Dimiev, A.; Kosynkin, D. V.; Sinitskii, A.; Slesarev, A.; Sun, Z.; Tour, J. M. Layer-by-Layer Removal of Graphene for Device Patterning. *Science* **2011**, *331*, 1168−1172.

(15) Prezioso, S.; Perrozzi, F.; Donarelli, M.; Bisti, F.; Santucci, S.; Palladino, L.; Nardone, M.; Treossi, E.; Palermo, V.; Ottaviano, L. Large Area Extreme-UV Lithography of Graphene Oxide via Spatially Resolved Photoreduction. *Langmuir* **2012**, *28*, 5489−5495.

(16) Ang, P. K.; Chen, W.; Wee, A. T. S.; Loh, K. P. Solution-Gated Epitaxial Graphene as pH Sensor. *J. Am. Chem. Soc.* **2008**, *130*, 14392−14393.

(17) Ohno, Y.; Maehashi, K.; Yamashiro, Y.; Matsumoto, K. Electrolyte-Gated Graphene Field-Effect Transistors for Detecting pH and Protein Adsorption. *Nano Lett.* **2009**, *9*, 3318−3322.

(18) Dong, X.; Shi, Y.; Huang, W.; Chen, P.; Li, L.-J. Electrical Detection of DNA Hybridization with Single-Base Specificity Using Transistors Based on CVD-Grown Graphene Sheets. *Adv. Mater.* **2010**, *22*, 1649−1653.

(19) Wang, Y.; Shao, Y.; Matson, D. W.; Li, J.; Lin, Y. Nitrogen-Doped Graphene and Its Application in Electrochemical Biosensing. *ACS Nano* **2010**, *4*, 1790−1798.

(20) Zhong, Z. Y.; Wu, W.; Wang, D.; Shan, J. L.; Qing, Y.; Zhang, Z. M. Nanogold-Enwrapped Graphene Nanocomposites as Trace Labels for Sensitivity Enhancement of Electrochemical Immunosensors in Clinical Immunoassays: Carcinoembryonic Antigen as a Model. *Biosens. Bioelectron.* **2010**, *25*, 2379−2383.

(21) Guo, C. X.; Ng, S. R.; Khoo, S. Y.; Zheng, X.; Chen, P.; Li, C. M. RGD-Peptide Functionalized Graphene Biomimetic Live-Cell Sensor for Real-Time Detection of Nitric Oxide Molecules. *ACS Nano* **2012**, DOI: 10.1021/nn301974u.

(22) Ratinac, K. R.; Yang, W.; Ringer, S. P.; Braet, F. Toward Ubiquitous Environmental Gas Sensors-Capitalizing on the Promise of Graphene. *Environ. Sci. Technol.* **2010**, *44*, 1167−1176.

(23) Schedin, F.; Geim, A. K.; Morozov, S. V.; Hill, E. W.; Blake, P.; Katsnelson, M. I.; Novoselov, K. S. Detection of Individual Gas Molecules Adsorbed on Graphene. *Nat. Mater.* **2007**, *6*, 652−655.

(24) Ao, Z. M.; Yang, J.; Li, S.; Jiang, Q. Enhancement of CO Detection in Al Doped Graphene. *Chem. Phys. Lett.* **2008**, *461*, 276−279.

(25) Chi, M.; Zhao, Y. P. Adsorption of Formaldehyde Molecule on the Intrinsic and Al-Doped Graphene: A First Principle Study. *Comput. Mater. Sci.* **2009**, *46*, 1085−1090.

(26) Zhang, Y. H.; Chen, Y. B.; Zhou, K. G.; Liu, C. H.; Zeng, J.; Zhang, H. L.; Peng, Y. Improving Gas Sensing Properties of Graphene by Introducing Dopants and Defects: A First-Principles Study. *Nanotechnology* **2009**, *20*, 185504.

(27) Robinson, J. T.; Perkins, F. K.; Snow, E. S.; Wei, Z. Q.; Sheehan, P. E. Reduced Graphene Oxide Molecular Sensors. *Nano Lett.* **2008**, *8*, 3137−3140.

(28) Fowler, J. D.; Allen, M. J.; Tung, V. C.; Yang, Y.; Kaner, R. B.; Weiller, B. H. Practical Chemical Sensors from Chemically Derived Graphene. *ACS Nano* **2009**, *3*, 301−306.

(29) Jung, I.; Dikin, D.; Park, S.; Cai, W.; Mielke, S. L.; Ruoff, R. S. Effect of Water Vapor on Electrical Properties of Individual Reduced Graphene Oxide Sheets. *J. Phys. Chem. C* **2008**, *112*, 20264−20268.

(30) Lu, G. H.; Ocola, L. E.; Chen, J. H. Gas Detection Using Low-Temperature Reduced Graphene Oxide Sheets. *Appl. Phys. Lett.* **2009**, *94*, 083111.

(31) Lu, G. H.; Ocola, L. E.; Chen, J. H. Reduced Graphene Oxide for Room-Temperature Gas Sensors. *Nanotechnology* **2009**, *22*, 445502.

(32) Mohanty, N.; Berry, V. Graphene-Based Single-Bacterium Resolution Biodevice and DNA Transistor: Interfacing Graphene Derivatives with Nanoscale and Microscale Biocomponents. *Nano Lett.* **2008**, *8*, 4469−4476.

(33) Cheng, R.; Liu, Y.; Ou, S.; Pan, Y.; Zhang, S.; Chen, H.; Dai, L.; Qu, J. Optical Turn-On Sensor Based on Graphene Oxide for Selective Detection of D-Glucosamine. *Anal. Chem.* **2012**, *84*, 5641−5644.

(34) Li, W.; Geng, X.; Guo, Y.; Rong, J.; Gong, Y.; Wu, L.; Zhang, X.; Li, P.; Xu, J.; Cheng, G. Reduced Graphene Oxide Electrically Contacted Graphene Sensor for Highly Sensitive Nitric Oxide Detection. *ACS Nano* **2011**, *5*, 6955−6961.

(35) He, Q.; Sudibya, H. G.; Yin, Z.; Wu, S.; Li, H.; Boey, F.; Huang, W.; Chen, P.; Zhang, H. Centimeter-Long and Large-Scale Micropatterns of Reduced Graphene Oxide Films: Fabrication and Sensing Applications. *ACS Nano* **2010**, *4*, 3201−3208.

(36) Han, T. H.; Huang, Y.-K.; Tan, A. T. L.; Dravid, V. P.; Huang, J. Steam Etched Porous Graphene Oxide Network for Chemical Sensing. *J. Am. Chem. Soc.* **2011**, *133*, 15264−15267.

(37) Li, F.; Xue, M.; Ma, X.; Zhang, M.; Cao, T. Facile Patterning of Reduced Graphene Oxide Film into Microelectrode Array for Highly Sensitive Sensing. *Anal. Chem.* **2011**, *83*, 6426−6430.

(38) Lu, G.; Park, S.; Yu, K.; Ruoff, R. S.; Ocola, L. E.; Rosenmann, D.; Chen, J. Toward Practical Gas Sensing with Highly Reduced Graphene Oxide: A New Signal Processing Method To Circumvent Run-to-Run and Device-to-Device Variations. *ACS Nano* **2011**, *5*, 1154−1164.

(39) Joshi, R. K.; Gomez, H.; Alvi, F.; Kumar, A. Graphene Films and Ribbons for Sensing of O_2, and 100 ppm of CO and NO_2 in Practical Conditions. *J. Phys. Chem.* **2010**, *114*, 6610−6613.

(40) Jeong, H. Y.; Lee, D.-S.; Choi, H. K.; Lee, D. H.; Kim, J.-E.; Lee, J. Y.; Lee, W. J.; Kim, S. O.; Choi, S.-Y. Flexible Room-Temperature NO_2 Gas Sensors Based on Carbon Nanotubes/Reduced Graphene Hybrid Films. *Appl. Phys. Lett.* **2010**, *96*, 213105.

(41) Deng, S.; Tjoa, V.; Fan, H. M.; Tan, H. R.; Sayle, D. C.; Olivo, M.; Mhaisalkar, S.; Wei, J.; Sow, C. H. Reduced Graphene Oxide Conjugated Cu_2O Nanowire Mesocrystals for High-Performance NO_2 Gas Sensor. *J. Am. Chem. Soc.* **2012**, *134*, 4905−4917.

(42) Chung, M. G.; Kim, D. H.; Lee, H. M.; Kim, T.; Choi, J. H.; Seo, D. K.; Yoo, J.-B.; Hong, S.-H.; Kang, T. J.; Kim, Y. H. Highly Sensitive NO_2 Gas Sensor Based on Ozone Treated Graphene. *Sens. Actuators B: Chem.* **2012**, *166 - 167*, 172−176.
(43) Tang, S.; Cao, Z. Adsorption of Nitrogen Oxides on Graphene and Graphene Oxides: Insights from Density Functional Calculations. *J. Chem. Phys.* **2011**, *134*, 044710.
(44) Treossi, E.; Melucci, M.; Liscio, A.; Gazzano, M.; Samorì, P.; Palermo, V. High-Contrast Visualization of Graphene Oxide on Dye-Sensitized Glass, Quartz, and Silicon by Fluorescence Quenching. *J. Am. Chem. Soc.* **2009**, *131*, 15576−15577.
(45) Liscio, A.; Veronese, G. P.; Tressi, E.; Suriano, F.; Rossella, F.; Bellani, V.; Rizzoli, R.; Samorì, P.; Palermo, V. Charge Transport in Graphene-Polythiophene Blends as Studied by Kelvin Probe Force Microscopy and Transistor Characterization. *J. Mater. Chem.* **2011**, *21*, 2924−2931.
(46) De Marco, P.; Nardone, M.; Vitto, A. D.; Alessandri, M.; Santucci, S.; Ottaviano, L. Rapid Identification of Graphene Flakes: Alumina Does It Better. *Nanotechnology* **2010**, *21*, 255703.
(47) Stankovich, S.; Dikin, A. D.; Piner, R. D.; Kohlhaas, K. A.; Kleinhammes, A.; Jia, Y.; Wu, Y.; Nguyen, S. T.; Ruoff, R. S. Synthesis of Graphene-Based Nanosheets via Chemical Reduction of Exfoliated Graphite Oxide. *Carbon* **2007**, *45*, 1558−1565.
(48) Park, S.; Lee, K. S.; Bozoklu, G.; Cai, W.; Nguyen, S. T.; Ruoff, R. S. Graphene Oxide Papers Modified by Divalent Ionsenhancing Mechanical Properties. *ACS Nano* **2008**, *2*, 572−578.
(49) Ren, P.-G.; Yan, D.-X.; Ji, X.; Chen, T.; Li, Z.-M. Temperature Dependence of Graphene Oxide Reduced by Hydrazine Hydrate. *Nanotechnology* **2011**, *22*, 055705.
(50) Perrozzi, F.; Prezioso, S.; Donarelli, M.; Bisti, F.; De Marco, P.; Santucci, S.; Nardone, M.; Treossi, E.; Palermo, V.; Ottaviano, L. Use of Optical Contrast to Estimate the Degree of Reduction of Graphene Oxide. *J. Phys. Chem. C* **2013**, *117*, 620−625.
(51) Estrade-Szwarckopf, H. XPS Photoemission in Carbonaceous Materials: A Defect Peak Beside the Graphitic Asymmetric Peak. *Carbon* **2004**, *42*, 1713−1721.
(52) Ferrari, A.; Robertson, J. Interpretation of Raman Spectra of Disordered and Amorphous Carbon. *Phys. Rev. B* **2000**, *61*, 14095−14107.
(53) Tuinstra, F.; Koenig, J. L. Raman Spectrum of Graphite. *J. Chem. Phys.* **1970**, *53*, 1126−1130.
(54) Mattevi, C.; Eda, G.; Agnoli, S.; Miller, S.; Mkhoyan, K. A.; Celik, O.; Mastrogiovanni, D.; Granozzi, G.; Garfunkel, E.; Chhowalla, M. Evolution of Electrical, Chemical, and Structural Properties of Transparent and Conducting Chemically Derived Graphene Thin Films. *Adv. Funct. Mater.* **2009**, *19*, 2577−2583.
(55) Kaiser, A. B.; Gómez-Navarro, C.; Sundaram, R. S.; Burghard, M.; Kern, K. Electrical Conduction Mechanism in Chemically Derived Graphene Monolayers. *Nano Lett.* **2009**, *9*, 1787−1792.
(56) Kong, J.; Franklin, N. R.; Zhou, C.; Chapline, M. G.; Peng, S.; Cho, K.; Dai, H. Nanotube Molecular Wires as Chemical Sensors. *Science* **2000**, *287*, 622−625.
(57) Crowther, A. C.; Ghassaei, A.; Jung, N.; Brus, L. E. Strong Charge-Transfer Doping of 1 to 10 Layer Graphene by NO_2. *ACS Nano* **2012**, *6*, 1865−1875.
(58) Nguyen, P.; Berry, V. Graphene Interfaced with Biological Cells: Opportunities and Challenges. *J. Phys. Chem. Lett.* **2012**, *3*, 1024−1029.
(59) Wang, H.; Wu, Y.; Cong, C.; Shang, J.; Yu, T. Hysteresis of Electronic Transport in Graphene Transistors. *ACS Nano* **2010**, *4*, 7221−7228.